IEEE Access
Multidisciplinary | Rapid Review | Open Access Journal

Received December 2, 2019, accepted December 20, 2019, date of publication January 1, 2020, date of current version January 15, 2020.

Digital Object Identifier 10.1109/ACCESS.2019.2963394

Analysis of the Harmonic Transmission Characteristics of HVDC Transmission Based on a Unified Port Theory Model

DUI LIU, XIAOHUA LI, (Member, IEEE), AND ZEXIANG CAI
School of Electric Power, South China University of Technology, Guangzhou 510640, China

Corresponding author: Xiaohua Li (eplxh@scut.edu.cn)

This work was supported by the Joint Fund Program of the National Nature Science Fund Program of China (U1766213) and the National Natural Science Foundation of China (51677073).

ABSTRACT The application of power electronics can introduce flexibility into power systems, but it can also cause harmonic problems. As a typical application of power electronics, high-voltage direct current (HVDC) transmission exhibits very prominent harmonic problems. In recent years, many HVDC protection maloperation events caused by harmonic problems have occurred in the field. The phenomena of harmonic transfer and amplification in HVDC transmission have an undeniable impact on the overall operation of a power system. Previous studies of these phenomena have relied mainly on detailed electromagnetic transient simulations. However, these simulations normally suffer from a large computational burden and low efficiency due to the complexity of the models and the small simulation time steps used. Therefore, an efficient analysis model of harmonics for various HVDC operating modes is presented in this paper. This model is based on port theory; every part of the HVDC transmission system is represented by an equivalent two-port component to construct a unified equivalent circuit. The proposed model is simple to calculate, and only the connections of the two-port components need to be changed to model different operation modes. The proposed two-port model is applied for the harmonic analysis of an HVDC transmission system, and the validity and accuracy of the model are confirmed by detailed electromagnetic simulations. Moreover, the model can be easily applied to HVDC systems for harmonic transfer and amplification, and the effects of the HVDC transmission power and smoothing reactor on harmonic transfer and amplification are analyzed.

INDEX TERMS HVDC transmission, harmonic modeling, two-port, operation model, harmonic transfer and amplification.

I. INTRODUCTION

The proportion of power electronics apparatuses in power systems has grown in recent years, and harmonic problems are becoming increasingly prominent in power systems [1]–[3]. For example, the harmonic problem of line-commutated converter high-voltage direct current (HVDC) transmission is particularly severe [4].

Recently, as an increasing number of HVDC transmission projects have been put into operation, the harmonic interaction between AC and DC systems and the transmission process of harmonics between AC and DC systems have become extremely complicated [5], [6]. In this case, the harmonics generated by AC-side faults or other behaviors of the AC/DC hybrid power grid may be transmitted to the DC side, causing maloperation of the harmonic protection system [7]–[10]. The phenomena of harmonic transfer and amplification in HVDC transmission have an undeniable impact on the operation of the overall power system [11], [12]. Many studies have been conducted on HVDC harmonics in academic and engineering circles. However, these studies have mainly focused on establishing an equivalent model that can accurately reflect the harmonics of the converter and determining how the interaction of AC-side harmonics and DC-side harmonics causes instability [13], [14]. The research on the harmonic calculation, transfer, and amplification of a detailed HVDC transmission system is insufficient [15], [16]. The stability of HVDC was analyzed in [17]–[19]; however, these

The associate editor coordinating the review of this manuscript and approving it for publication was Lei Jiao.

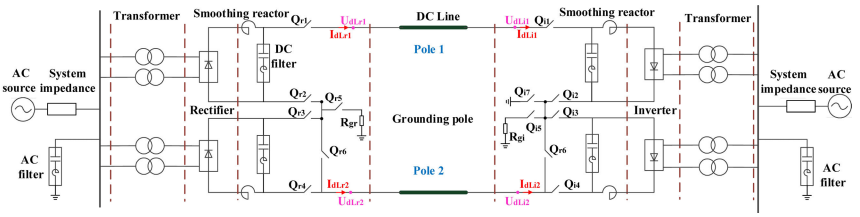

FIGURE 1. HVDC system circuit diagram.

analyses rely on small signal models and do not pay much attention to harmonic problems. Based on a dynamic phasor model, the harmonics of a DC system under asymmetric faults were calculated in [20]–[22]; however, the study did not analyze harmonic transfer and amplification in detail. A switching function model was used to calculate the harmonics and inter-harmonics of DC systems for weak AC systems in [23], but the model was a back-to-back model and did not consider DC lines. A new approach for modeling line-commutated AC/DC/AC conversion systems based on modulation function theory was presented and discussed in [24]. This new approach considers the DC-side harmonics caused by the impedance time variance. However, a solution of the time-varying impedance was not given in the paper, and the influence of the line was not considered. A method for directly calculating the harmonic current flowing through a DC conductor and a grounding conductor and the harmonic current induced in the DC side and grounding conductors was proposed in [25]; however, the paper did not consider the different operating modes of the HVDC system. A DC system model and transmission line model were established to analyze the DC harmonics in [26]; this calculation method can effectively calculate the harmonics on the DC side, but the model of the DC line is too simple, and the harmonic calculation method is only for a certain operation mode of the HVDC system. An HVDC harmonic domain model was presented in [27]. The HVDC link was also modeled with an extended control system for a realistic specification of the steady-state operating point. The Newton method, which requires a high initial value and may not converge, was used to solve the problem. In the abovementioned research, a model of the converter was established, and the harmonics on the DC side were calculated. However, the DC line model is not considered adequately, and the operation of the HVDC system is not considered in the analysis of the harmonics.

In this paper, a detailed two-port analysis model of an HVDC transmission system is presented. To cover the different HVDC operation modes, the HVDC system is modeled in detail, including DC smoothing reactors and filters. These complex situations were not modeled in the work presented above. In the two-port model proposed in this paper, the transformer, converter, smoothing reactor and filter, and DC line in the HVDC transmission system are equivalent to one two-port network. The connection of the two ports of each part forms a whole two-port network. According to the different operation modes of HVDC transmission, only the connection mode of the two-port part needs to be modified, and the other parts remain unchanged [28], [29]. In this way, HVDC transmission forms a unified two-port network under different operation modes. After verifying the accuracy of the established model, the phenomena of harmonic transfer and amplification in HVDC transmission are analyzed. This paper also presents an analysis to show the influence of the HVDC transmission power and smoothing reactor on harmonic transmission and amplification.

This paper is organized as follows. Section II describes the HVDC transmission system and the whole equivalent two-port network. The specific equivalent model of the converter and the DC line are described in detail in Section III. Section IV describes the equivalent method of the different connections of the two ports and the port processing of the HVDC in different operating modes. Section V presents a case study and discussion comparing the processing results of the proposed model with those of the PSCAD/EMTDC and then analyzes the harmonic transmission characteristics. The conclusions are given in section VI.

II. HVDC TRANSMISSION SYSTEM

The typical schematic diagram of an HVDC transmission system is shown in FIGURE 1. In this diagram, U stands for the voltage, I stands for the current, and Q represents the connection switch. The subscript r stands for the rectifier side, the subscript i stands for the inverter side, the subscript 1 stands for pole 1, and the subscript 2 stands for pole 2. R_{gr} and R_{gi} represent the grounding electrode resistances of the rectifier side and the inverter side, respectively. The representation in the following figure is similar.

According to the components, the HVDC transmission is divided into different parts. The dashed lines in the schematic are represented as a two-port network. The specific equivalent circuit inside each two-port network will be described in the following sections. In this way, the operation of HVDC transmission is associated with the different connections of the two-port network. The two-port equivalent schematic is shown in FIGURE 2.

Based on the principle of HVDC transmission, the AC system is connected to the end of the port. With the two-port equivalent circuit, the node admittance matrix Y of the circuit can be obtained. The Norton equivalent principle is used to

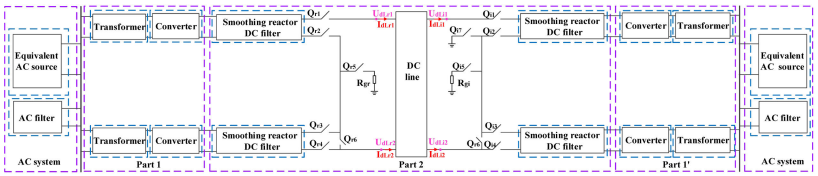

FIGURE 2. The two-port equivalent schematic diagram.

equate the harmonic voltage source to the harmonic injection current I; the solution of $YU = I$ can provide the voltage of the corresponding node so that the corresponding current value can be obtained.

III. COMPONENT EQUIVALENT MODEL

To obtain the equivalent circuit of the HVDC transmission, it is necessary to model each part to obtain its corresponding two-port network.

A. SWITCHING FUNCTION MODEL

Modulation theory is applied to study the converters of an HVDC transmission system because of its clear physical concept, simple calculation process, and high precision. The basic principle is to regard the converter as a modulation switch circuit for connecting the DC and AC systems [2], [30]. The voltage and current in the AC/DC system can be converted accordingly by the modulated switching function.

According to the working principle of the switching function, the relationship between the DC voltage and current and the AC voltage and current in different states of the converter can be described. For the 6-pulse converter shown in FIGURE 3, the expression is given by equations (1) and (2):

$$U_d = u_a S_{ua} + u_b S_{ub} + u_c S_{uc} \tag{1}$$

$$\begin{cases} i_a = I_d S_{ia} \\ i_b = I_d S_{ib} \\ i_c = I_d S_{ic} \end{cases} \tag{2}$$

where U_d and I_d are the DC-side voltage and current, respectively; u_a, u_b, u_c and i_a, i_b, i_c represent the three-phase voltage and current on the AC side, respectively; S_{ua}, S_{ub}, S_{uc} represent the ABC three-phase voltage switch functions; and S_{ia}, S_{ib}, S_{ic} represent the ABC three-phase current switch functions.

In general, trigger pulses of HVDC systems are generated at equal intervals. In harmonic analysis, the switching

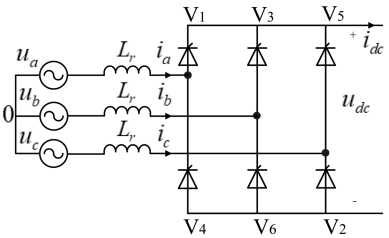

FIGURE 3. A schematic diagram of the 6-pulse converter.

function of the voltage and current modulation of the converter can be decomposed into a Fourier series based on theory. For a 6-pulse converter, the switching function can be expressed by equation (3):

$$\begin{cases} S_a = \sum_{n=1}^{\infty} A_n \cos n\omega t \\ S_b = \sum_{n=1}^{\infty} A_n \cos(n\omega t - \frac{2\pi n}{3}) \quad n = 1, 3, 5 \cdots \\ S_c = \sum_{n=1}^{\infty} A_n \cos(n\omega t + \frac{2\pi n}{3}); \end{cases} \tag{3}$$

In the above expressions, A_n is a coefficient and ω is the angular frequency.

The phase voltage switching function and current switching function of the 6-pulse converter are shown in FIGURE 4. S_a is the switching function without considering the commutation process. S_{ua} is the voltage switching function considering the commutation process, and S_{ia} is the current switching function considering the commutation process [15], [31].

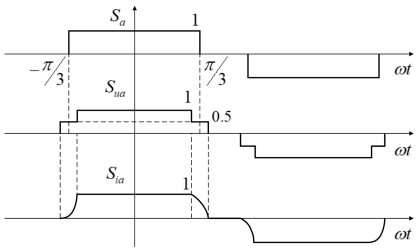

FIGURE 4. Graphic of the switching function.

When the commutation angle μ is neglected, the expression of the coefficient is:

$$\begin{aligned} A_n &= \frac{2}{\pi}\int_0^{\pi} f(x)\cos nxdx \\ &= \frac{2}{\pi}(\int_0^{\pi/3} \cos nxdx - \int_{2\pi/3}^{\pi} \cos nxdx) \\ &= \frac{4}{n\pi}\sin\frac{n\pi}{2}\cos\frac{n\pi}{6} \end{aligned} \tag{4}$$

When the commutation angle μ is considered, the expression of the coefficient is:

$$\begin{aligned} A_{nu} &= \frac{2}{\pi}(\int_0^{\pi/3-\mu/2} \cos nxdx + \int_{\pi/3-\mu/2}^{\pi/3+\mu/2} \cos nxdx \\ &\quad - \int_{2\pi/3-\mu/2}^{2\pi/3+\mu/2} \cos nxdx - \int_{2\pi/3+\mu/2}^{\pi} \cos nxdx) \\ &= A_n \cos\frac{n\mu}{2} \end{aligned} \tag{5}$$

$$A_{ni} = \frac{2}{\pi}\left\{\begin{array}{l}\int_0^{\pi/3-\mu/2}\cos nxdx - \int_{2\pi/3+\mu/2}^{\pi}\cos nxdx \\ +\int_{\pi/3-\mu/2}^{\pi/3+\mu/2}(-\frac{x}{\mu}+\frac{\pi}{3\mu}+\frac{1}{2})\cos nxdx \\ +\int_{2\pi/3-\mu/2}^{2\pi/3+\mu/2}(-\frac{x}{\mu}+\frac{\pi}{3\mu}+\frac{1}{2})\cos nxdx\end{array}\right\} = A_n \sin\frac{n\mu}{2}/\frac{n\mu}{2} \quad (6)$$

On the basis of the switching function model of the converter, the harmonics caused by the harmonic voltage from the AC side to the DC side will be analyzed. Take the 6-pulse converter as an example. Consider the general case where the AC bus of the converter has a voltage with a frequency of f; its expression is:

$$\left\{\begin{array}{l} u_{af} = U_f\cos(\omega_f t + \theta_f) \\ u_{bf} = U_f\cos(\omega_f t + \theta_f - \frac{2\pi}{3}) \\ u_{cf} = U_f\cos(\omega_f t + \theta_f + \frac{2\pi}{3}) \end{array}\right. \quad (7)$$

where U_f is the amplitude of the AC-side voltage and θ_f is the corresponding initial phase angle.

As explained in [32] and [33], research on the harmonics of the DC system shows that the non-characteristic harmonic voltage of $n > 1$ is an order of magnitude lower than the non-characteristic harmonic voltage of $n = 1$ for 12-pulse converters. Therefore, considering only the lower order non-characteristic harmonic voltages would be adequate for industry practice.

By substituting equation (7) into equation (1), a dominant harmonic voltage with a frequency of $(f_f - f_1)$ is produced on the DC side after the converter modulation:

$$E^{+}_{dc(f-f_1)} = \frac{3}{2}A_{nu}U_f\cos\left[(\omega_f-\omega_1)t+\theta_f\right] = \frac{3\sqrt{3}}{\pi}\cos\frac{\mu}{2}\times U_f\cos\left[(\omega_f-\omega_1)t+\theta_f\right] \quad (8)$$

The analysis of equation (8) indicates that if there is a positive second-order harmonic voltage disturbance in the AC system, the number of harmonic components generated on the DC side will be reduced by 1 after the corresponding modulation effect of the converter. That is, a 50Hz voltage component with an amplitude of $\frac{3\sqrt{3}}{\pi}\cos\frac{\mu}{2}\times U_f$ can be obtained.

Similarly, if the DC current of the converter is:

$$I_{dch} = I_{dc}\cos(\omega t + \varphi) \quad (9)$$

where I_{dc} is the amplitude of the small signal on the DC-side and φ is the corresponding initial phase angle, then the AC-side three-phase current expression can be obtained by applying equation (2) for the corresponding calculation.

It can be seen from equation (10) that the DC-side small signal I_{dch} will generate two sets of dominant uncharacteristic harmonics on the AC side, one of which has a positive sequence and an angular frequency of $\omega+\omega_1$. $\varphi_a, \varphi_b, \varphi_c$ are the angles of other components.

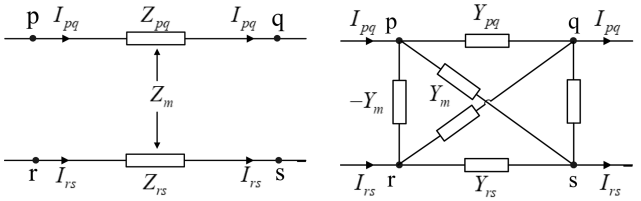

(a) Mutual inductance lines (b) Equivalent circuits

FIGURE 5. Two mutual inductance lines and their equivalent circuits.

$$\left\{\begin{array}{l} i_a = I_{dch}S_{ia} = \frac{1}{2}A_{ni}I_{dc}\left\{\cos\left[(\omega+\omega_1)t+\varphi\right]+\cos\varphi_a\right\} \\ i_b = I_{dch}S_{ib} = \frac{1}{2}A_{ni}I_{dc} \\ \qquad \times\left\{\cos\left[(\omega+\omega_1)t+\varphi-\frac{2\pi}{3}\right]+\cos\varphi_b\right\} \\ i_c = I_{dch}S_{ic} = \frac{1}{2}A_{ni}I_{dc} \\ \qquad \times\left\{\cos\left[(\omega+\omega_1)t+\varphi+\frac{2\pi}{3}\right]+\cos\varphi_c\right\} \end{array}\right. \quad (10)$$

Therefore, if there is a current of 50Hz on the DC side of the converter, and a 100Hz current with an amplitude of $\frac{2\sqrt{3}}{\pi\mu}\sin\frac{\mu}{2}\times I_{dc}$ will be generated in the AC system.

B. DC LINE MODEL

An actual HVDC transmission line generally consists of multiple parallel wires. The frequency-dependent model [34], [35] is used in this paper. There is electromagnetic coupling between the wires, and the electromagnetic process is complex. Therefore, the wires should be decoupled.

In the frequency-dependent model, modal decoupling is usually carried out by means of Clarke's matrix or a modal representation using a propagation matrix. However, the question of how to deal with the coupling relationship between two lines after those lines are connected to external components has not been studied. To adapt to the different operating modes of the HVDC transmission system, a unified model of the DC lines should be established. The key point is how to solve for the coupling between the lines. Therefore, a method based on the elimination of mutual inductance is used in this paper to construct a unified two-port matrix of the HVDC transmission system lines in different operation modes. Two mutual inductance branches are taken as examples to illustrate the principle of removing the mutual inductance between the phases, as shown in FIGURE 5.

The branch voltage equation of the two mutual inductance branches shown in FIGURE 5 (a) can be expressed by a matrix as follows:

$$\begin{bmatrix}\dot{U}_p-\dot{U}_q \\ \dot{U}_r-\dot{U}_s\end{bmatrix} = \begin{bmatrix} z_{pq} & z_m \\ z_m & z_{rs}\end{bmatrix}\begin{bmatrix}\dot{I}_{pq} \\ \dot{I}_{rs}\end{bmatrix} \quad (11)$$

By a transformation, the following can be obtained:

$$\begin{bmatrix} \dot{I}_{pq} \\ \dot{I}_{rs} \end{bmatrix} = \begin{bmatrix} y'_{pq} & y'_m \\ y'_m & y'_{rs} \end{bmatrix} \begin{bmatrix} \dot{U}_p - \dot{U}_q \\ \dot{U}_r - \dot{U}_s \end{bmatrix} \tag{12}$$

where

$$\begin{cases} y'_{pq} = \dfrac{z_{rs}}{z_{rs}z_{pq} - z_m^2} \\ y'_{rs} = \dfrac{z_{pq}}{z_{rs}z_{pq} - z_m^2} \\ y'_m = \dfrac{z_m}{z_{rs}z_{pq} - z_m^2} \end{cases}$$

According to the above equation, a nonmutual inductance equivalent circuit with the mutual inductance eliminated can be made, as shown in FIGURE 5(b). The equivalent circuit is a noninductive circuit consisting of four nodes and six branches. The admittance values of each branch are y'_{pq}, y'_m, and y'_{rs}.

Through the equivalent circuit without mutual inductance, it is convenient to use the node voltage method to obtain the corresponding node voltage equations as:

$$\begin{bmatrix} \dot{I}_{pq} \\ \dot{I}_{rs} \\ \dot{I}_{qp} \\ \dot{I}_{sr} \end{bmatrix} = \begin{bmatrix} y'_{pq} & y'_m & -y'_{pq} & -y'_m \\ y'_m & y'_{rs} & -y'_m & -y'_{rs} \\ -y'_{pq} & -y'_m & y'_{pq} & y'_m \\ -y'_m & -y'_{rs} & y'_m & y'_{rs} \end{bmatrix} \begin{bmatrix} \dot{U}_p \\ \dot{U}_r \\ \dot{U}_q \\ \dot{U}_s \end{bmatrix} \tag{13}$$

C. HVDC CONTROL SYSTEM

The ability to achieve multiple fast modes of regulation is one of the main advantages of HVDC systems. The operating point of the HVDC system can be changed by adjusting the firing angle of the converter valve or the ratio of the converter transformer according to the operating conditions of the AC/DC system.

Normally, the HVDC rectifier side achieves constant current control by reducing the firing angle. Different from the rectifier side, the inverter side usually adopts both constant arc extinction angle control and constant current control [36]-[38]. The overall control scheme is shown in FIGURE 6. In the figure, $I_{\text{d-rec}}$ and I_{dec} represent the measured value and reference value, respectively, of the rectifier side current; $U_{\text{d-inv}}$ and $I_{\text{d-inv}}$ are the measured values of the voltage and current, respectively, on the inverter side; γ_y and γ_d are the measured values of the arc extinction angles of the Y-bridge and D-bridge, respectively, on the inverter side; γ_{ord} is the inverter side arc extinction angle reference value; and α_{rec} and α_{inv} are the rectifier side and inverter side firing angles, respectively, of the control output.

The control system shown in FIGURE 6 is used in the CIGRE HVDC benchmark system [36], [37] and is also used in the case studies in this paper.

Modern HVDC systems generally adopt the equal-interval triggering mode, which is followed by the phase locked loop (PLL) to generate the synchronous sawtooth signal. According to the PLL following phase, six equally spaced pulse signals will be generated when the sawtooth signal is reset and compared with the trigger angle pulse signal of the pole control layer to realize the trigger command to the valve [19], [39].

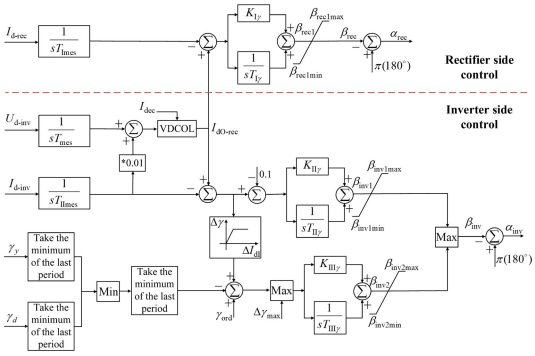

FIGURE 6. HVDC control scheme.

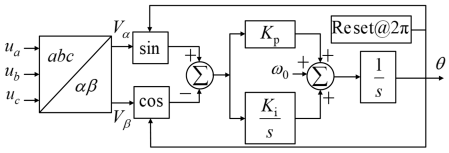

FIGURE 7. Phase locked loop model.

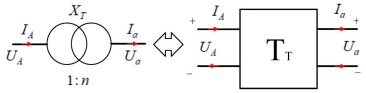

FIGURE 8. Equivalent two-port diagram for the transformer.

The control block diagram of the PLL is shown in FIGURE 7. In the figure, u_a, u_b, and u_c are the input AC voltages; the output is the following phase θ. K_{p} and K_{i} are the parameters of the control part [19]. The control system parameters are shown in APPENDIX A.

IV. TWO-PORT CONNECTION

To obtain the overall equivalent circuit, it is necessary to determine the connection relationship of each two-port network.

A. EQUIVALENT TWO-PORT NETWORK FOR THE TRANSFORMER AND CONVERTER UNION

Taking Y-y as an example, if the converter transformer is equivalent to a two-port network, then the equivalent diagram is shown in FIGURE 8. In the figure, U_A and I_A are the primary-side voltage and current, respectively; U_a and I_a are the secondary-side voltage and current, respectively; n is the transformer ratio; and X_T is the leakage inductance of the transformer [40]. When other connections are adopted for the transformer, the derivation is similar.

According to the corresponding relationship of the transformer ratio, the T-parameter of the equivalent port of the

transformer can be obtained.

$$\begin{bmatrix} \dot{\boldsymbol{U}}_A \\ \dot{\boldsymbol{I}}_A \end{bmatrix} = \begin{bmatrix} T_{T11} & T_{T12} \\ T_{T21} & T_{T22} \end{bmatrix} \begin{bmatrix} \dot{\boldsymbol{U}}_a \\ \dot{\boldsymbol{I}}_a \end{bmatrix} \tag{14}$$

In the above conversion,

$$\begin{cases} T_{T11} = 1/n \\ T_{T12} = -n * Z_T \\ T_{T21} = 0 \\ T_{T22} = -n \end{cases}$$

Here, Z_T is the transformer leakage inductance at the corresponding frequency.

Similarly, the 6-pulse converter is treated as a port, as shown in FIGURE 9. In the figure, U_{acp} and I_{acp} are the AC-side voltage and current, and U_{dch} and I_{dch} are the DC-side voltage and current, respectively.

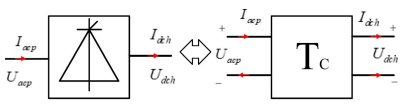

FIGURE 9. Equivalent two-port diagram of the 6-pulse converter.

From the analysis in the previous section, equations (8) and (10) are the correspondence between AC and DC. Using the relationship between the AC and DC sides of the converter, when $n = 1$, the T-parameter of the equivalent two-port circuit of the converter can be obtained [41].

$$\begin{bmatrix} \dot{\boldsymbol{U}}_{dch} \\ \dot{\boldsymbol{I}}_{dch} \end{bmatrix} = \begin{bmatrix} T_{C11} & T_{C12} \\ T_{C21} & T_{C22} \end{bmatrix} \begin{bmatrix} \dot{\boldsymbol{U}}_{ach} \\ \dot{\boldsymbol{I}}_{ach} \end{bmatrix} \tag{15}$$

In the above formula,

$$\begin{cases} T_{C11} = 1/(\dfrac{3\sqrt{3}}{\pi} \cos \dfrac{\mu}{2}) \\ T_{C12} = 0 \\ T_{C21} = 0 \\ T_{C22} = -\dfrac{2\sqrt{3}}{\pi \mu} \sin \dfrac{\mu}{2} \end{cases}$$

The two two-port cascades of the transformer and inverter are shown in FIGURE 10.

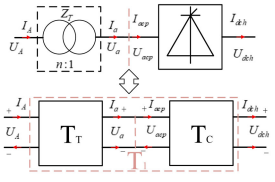

FIGURE 10. Two-port network cascading.

The equivalent expressions of the two cascaded ports can be obtained by using the basic principle of circuit theory [41].

$$\boldsymbol{T}_1 = \boldsymbol{T}_T * \boldsymbol{T}_C \tag{16}$$

In the above equation, T_T and T_C represent the T-parameters of the first and second two-port networks, respectively. T_1 is the T-parameter after the two-port networks are cascaded. In this way, for 6-pulse HVDC transmission, the equivalent two-port parameters of the transformer and the converter can be obtained.

In addition, 12-pulse HVDC transmission is equivalent to a combination of two 6-pulse systems, as shown in FIGURE 11.

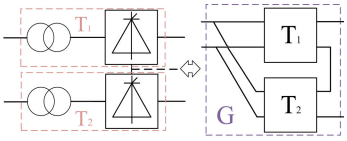

FIGURE 11. Two-port network in parallel and in series.

To facilitate the calculation, the T-parameter of the two ports must be converted into the corresponding G-parameter. If the T-parameter of the two-port network is assumed to be equation (17), then the two-port G-parameter can be obtained.

$$\boldsymbol{T}_0 = \begin{bmatrix} T_A & T_B \\ T_C & T_D \end{bmatrix} \tag{17}$$

$$\boldsymbol{G}_0 = \frac{1}{T_A} \begin{bmatrix} T_C & -\Delta T \\ 1 & T_B \end{bmatrix} \tag{18}$$

In the equation, $\Delta T = T_A T_D - T_B T_C$.

Using the change of formulas (17) and (18), the G-parameters of the two two-port networks corresponding to the 12-pulse system can be obtained.

Two two-port networks are connected in parallel on the left side and in series on the right side. The connection parameters can be obtained using equation (19).

$$\boldsymbol{G} = \boldsymbol{G}_1 + \boldsymbol{G}_2 \tag{19}$$

The inverter side adopts a similar method; the only difference is that the port connection is different.

B. DIFFERENT OPERATION MODES

There are several typical modes of operation for HVDC transmission [28]. By changing the different combinations in Part 2 of FIGURE 2, it is possible to construct different operation modes.

The wiring diagram of Part 2 for bipolar ground operation mode is shown in FIGURE 12(a). It can be seen from the figure that the two poles are symmetrical when operating in bipolar ground mode, and the voltage on the ground electrode is zero. The monopolar ground operation mode requires a modification of the partial wiring, as shown in FIGURE 12(b). In the monopolar ground operation mode, the pole 2 DC line is disconnected from the connected smoothing reactor. Although only one DC line is in operation, the circuit structure of the rectifier side and the inverter side are still symmetrical. When the HVDC system is in the monopolar metallic operation mode, the wiring of Part 2 is shown in FIGURE 12(c). It can be seen from the figure that the pole 2 DC line is directly connected to the smoothing reactor of pole 1. In addition, the rectifier side and the inverter

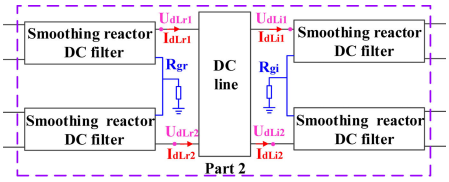

(a) Partial two-port equivalent wiring schematic diagram of the bipolar ground operation mode

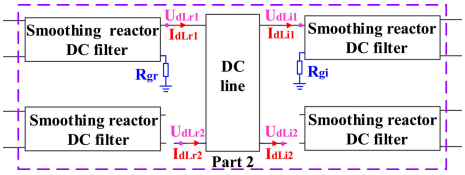

(b) Partial two-port equivalent wiring schematic diagram of the monopolar ground operation mode

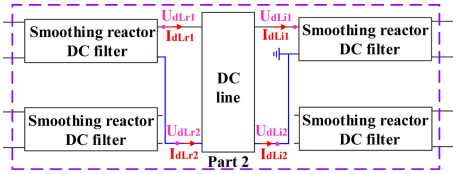

(c) Partial two-port equivalent wiring schematic diagram of the monopolar metallic operation mode

FIGURE 12. Partial two-port network.

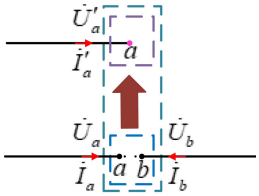

FIGURE 13. Node combination diagram.

side are asymmetrical at this time, mainly because there is a grounding point on the inverter side.

C. PORT CONSOLIDATION AND PORT GROUNDING PROCESSING IN DIFFERENT OPERATION MODES

Although HVDC transmission has different modes of operation, when forming the equivalent matrix, it is only necessary to modify the corresponding part of the matrix according to different port connections.

1) PORT CONSOLIDATION

The two ports of the transformer and converter are described in the previous sections, and the port of the DC line is also explained in detail. The admittance matrix is used when the port is connected by a node [42], [43]. The node combination is shown in FIGURE 13.

When two nodes are combined into one node, the injection current of the new node is equal to the sum of the injection currents of the original two nodes. For example, for the node a, b combination, the merged node becomes a, and so there is $\dot{U}_a + \dot{U}_b = \dot{U}'_a$ and $\dot{I}_a + \dot{I}_b = \dot{I}'_a$; the superscript‘’ indicates a

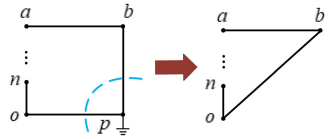

FIGURE 14. Node elimination diagram.

new value. At this time, the network equation will be reduced by one order. If $\dot{U}_a$ is replaced by $\dot{U}'_a$, then $\dot{U}_a$ is eliminated; $\dot{I}_a$ is replaced by $\dot{I}'_a$, and $\dot{I}_a$ is eliminated. Correspondingly, the bth row of the admittance matrix is added to the a row, and the bth column is added to the a column. In this way, the connected port admittance matrix can be obtained.

2) PORT GROUNDING

The port needs to eliminate these nodes when the grounding point occurs [43]. Assuming that node p is the node to be erased and node p is given later, the network equation represented by the admittance matrix is used. The expression after matrix partitioning is given by equation(20).

$$\begin{bmatrix} \boldsymbol{Y}_{\mathrm{I}} & \boldsymbol{Y}_{\mathrm{II}} \\ \boldsymbol{Y}_{\mathrm{III}} & Y_{\mathrm{IV}} \end{bmatrix} \begin{bmatrix} \dot{\boldsymbol{U}}_n \\ \dot{U}_p \end{bmatrix} = \begin{bmatrix} \dot{\boldsymbol{I}}_n \\ \dot{I}_p \end{bmatrix} \tag{20}$$

After eliminating node p, the following formula can be obtained:

$$(\boldsymbol{Y}_{\mathrm{I}} - \boldsymbol{Y}_{\mathrm{II}} Y_{\mathrm{IV}}^{-1} \boldsymbol{Y}_{\mathrm{III}}) \dot{\boldsymbol{U}}_n = \dot{\boldsymbol{I}}_n - \boldsymbol{Y}_{\mathrm{II}} Y_{\mathrm{IV}}^{-1} \dot{I}_p \tag{21}$$

Equation (21) is the node admittance matrix after node p is eliminated, and its corresponding diagram is shown in FIGURE 14.

V. CASE STUDY AND DISCUSSION

In this section, two case studies with an analysis and a discussion are presented. Section A is mainly used to prove the accuracy of the model. Section B uses the verified model to analyze harmonic transfer and amplification, and this part focuses on the analysis of the HVDC transmission power and the effect of the DC reactor on harmonic transmission and amplification.

A. HARMONIC QUANTITATIVE CALCULATION ANALYSIS

This section is divided into two parts to verify the accuracy and validity of the two-port model. The first part uses the CIGRE HVDC benchmark system, and the second part uses the actual engineering model.

1) THE CIGRE HVDC BENCHMARK SYSTEM MODEL

To verify the effectiveness of the proposed method, the line of the CIGRE HVDC benchmark system was changed to the double coupled line, and the line length was 1254 km. The tower structure of DC line is shown in APPENDIX B. The model of the modified CIGRE HVDC benchmark system based on the two-port model was developed in MATLAB.

Taking the positive sequence 2nd harmonic of the rectifier-side AC system as an example, an 8% (24.24 kV) harmonic

source was added to the AC system. The simulation and calculation were performed on a computer with a 3.40 GHz i7-6700 processor, 8 GB of RAM memory, and the 64-bit version of Windows 10. The computation (CPU) time required by the methods was recorded. The calculated value of the equivalent circuit was compared with the simulated value of PSCAD/EMTDC, as shown in TABLE 1.

TABLE 1. Comparison of the harmonic calculation and simulation values.

Method	UdLr1/kV	IdLr1/A	UdLi1/kV	IdLi1/A	Total time/s
Simulated value	33.7497	43.3722	10.3549	87.4157	12.4000
Calculated value	35.3630	39.5130	10.9710	94.4309	1.0370
Relative error /%	4.7803	8.8980	5.9503	8.0250	/
Speed-up gain	/	/	/	/	12.4/1.037 =11.9576

TABLE 1 shows that the CPU time required by the proposed method is shorter than that required by the simulation method, and the proposed method can offer simulation-level accuracy with a marked reduction in computing burden. However, the CIGRE HVDC benchmark system has certain limitations in terms of the AC filters. Therefore, the following simulation in this manuscript uses the actual engineering model.

2) THE ACTUAL ENGINEERING MODEL

Based on the PSCAD/EMTDC platform, combined with a ±500kV HVDC transmission engineering model, a simulation is carried out. The specific parameters of the model are shown in APPENDIX C.

Taking the positive sequence 2nd harmonic of the rectifier-side AC system as an example, a 9% (27.27 kV) harmonic source is added to the AC system. When the HVDC system operates in bipolar ground mode, the simulation value of the 50Hz harmonic voltage and current can be obtained by measuring the corresponding node. Similarly, the same harmonic is added to the rectifier-side AC system, and the calculated value of the 50Hz harmonic can be obtained by the corresponding calculation. The calculated value of the equivalent circuit is compared with the simulated value of PSCAD/EMTDC in TABLE 2.

Comparing the data, it can be found that the calculated values of the voltage and current of the DC line are close to the simulated values when the HVDC system is in three different operation modes; the relative error is small, which indicates the harmonic calculation method is accurate.

To verify the applicability of the model, the accuracy of the model for different degrees of harmonics is considered below. After the model is stably operated, 1%–19% of the phase voltage is superimposed on the rectifier side, and the interval is 2%. The voltage and current on both sides are recorded. The rectifier-side calculated value (RCV), the rectifier-side simulated value (RSV), the inverter-side calculated value (ICV) and the inverter-side simulated value (ISV) are compared.

TABLE 2. Comparison of the harmonic calculation and simulation values.

Mode	Voltage, Current	Calculated value	Simulated value	Relative error /%
Bipolar ground operation mode	UdLr1/kV	41.5361	41.8945	0.8556
	IdLr1/A	18.2046	19.8143	8.1224
	UdLi1/kV	19.7580	21.0356	6.0732
	IdLi1/A	144.0716	146.5659	1.7018
Monopolar ground operation mode	UdLr1/kV	42.0106	40.3642	4.0789
	IdLr1/A	44.6025	42.6339	4.6173
	UdLi1/kV	18.2185	19.1937	5.0820
	IdLi1/A	111.0193	108.3051	2.5061
Monopolar metallic operation mode	UdLr1/kV	30.3392	31.1147	2.4922
	IdLr1/A	14.1777	14.8119	4.2815
	UdLi1/kV	12.3170	13.3455	7.7061
	IdLi1/A	95.6147	99.1634	3.5786

The voltage and current of the RCV, RSV, ICV, and ISV of the bipolar ground operation mode are shown in FIGURE 15. The details of the other two operating modes are shown in APPENDIX D.

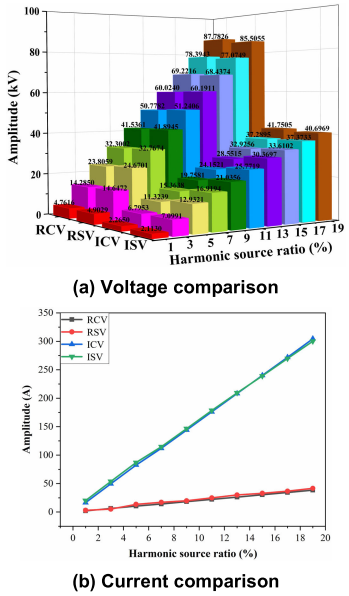

(a) Voltage comparison

(b) Current comparison

FIGURE 15. Comparison of the bipolar ground operation mode.

It can be seen from the comparison in the figure that the calculated value is very similar to the simulated value. Thus, the model still has high accuracy for different degrees of harmonics.

TABLE 3. Current transfer for different transmission powers.

Power/ p.u.	CV/SV	Rectifier-side I/A	Inverter-side I/A	Amplification factor
0.1	CV	41.0698	102.9082	2.5056
	SV	40.1871	102.8329	2.5588
0.3	CV	42.3111	105.1921	2.4862
	SV	40.3107	105.5928	2.6194
0.5	CV	43.1159	107.3360	2.4895
	SV	40.0962	106.5814	2.6581
0.7	CV	44.1337	109.6798	2.4851
	SV	41.0962	106.6094	2.5941
0.9	CV	44.0382	109.6264	2.4893
	SV	41.3988	107.7290	2.6022

TABLE 4. Current transfer for different smoothing reactors.

L/H	CV/SV	Rectifier-side I/A	Inverter-side I/A	Amplification factor
0.25	CV	10.3706	95.6181	9.2201
	SV	11.0119	99.3335	8.9935
0.30	CV	14.1777	95.6147	6.7440
	SV	14.8119	99.1634	6.6948
0.35	CV	18.3562	96.2338	5.2426
	SV	19.8986	101.6241	5.1070
0.40	CV	22.785	97.1247	4.2629
	SV	23.3067	103.1825	4.4271

In addition, it can be seen intuitively from the figure that, as the harmonic source increases, both the voltage component and the current component increase in the rectifier side or the inverter side. The current component is amplified by the transmission of the line; the voltage component is reduced by the line transmission. Therefore, it is necessary to pay special attention to the amplified component of the DC current transmitted to the opposite side. The size of this current component largely determines whether the protection will malfunction.

B. HARMONIC TRANSFER AND AMPLIFICATION

In this section, the above-described verified model is used to analyze the effects of different quantities on harmonic transmission, with a focus on the amplification of the current transfer to the opposite side. The amplification factor is defined as the ratio of the terminal harmonic amplitude to the terminal harmonic amplitude.

The proposed model can be used to analyze the relationship between the DC current amplification factor and the operating and system parameters. The HVDC transmission power and the DC smoothing reactor will be analyzed as an example.

TABLE 5. Control system parameters.

Controller	Parameter	Rectifier	Inverter
Current controller	Proportional gain	1.0989	0.63
	Integral gain	0.01092	0.01524
Arc extinction angle control	Proportional gain	/	0.7506
	Integral gain	/	0.0544
Current measurement	Integral gain	0.0012	0.0012
Voltage measurement	Integral gain	/	0.02
Phase locked loop	Proportional gain	10	10
	Integral gain	50	50

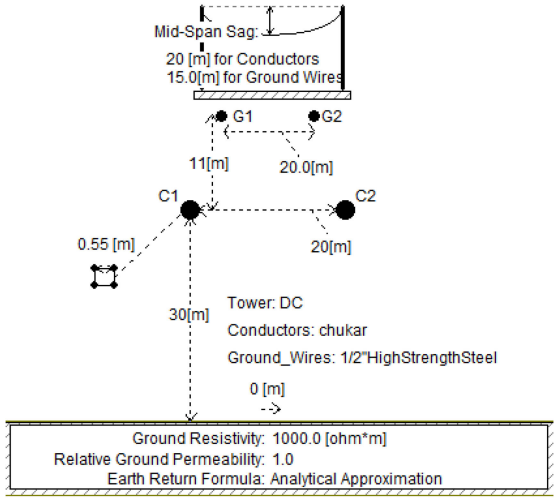

FIGURE 16. Tower structure of HVDC transmission lines.

TABLE 6. The parameters of the simulation model.

Parameter	Value
Rated capacity	3200MW
Rated voltage	±500kV
DC line	1254 km
Rectifier-side AC system	4.58228∠86.002°
Inverter-side AC system	5.7735∠81.776°
Rectifier-side leakage reactance	0.165 p.u.
Inverter-side leakage reactance	0.165 p.u.
Rectifier-side transformer capacity	952.8 MVA
Inverter-side transformer capacity	907.5 MVA

The results will not only show the characteristics of the harmonic transfer and amplification but also illustrate the accuracy of the two-port model.

1) HVDC TRANSMISSION POWER

In actual operation, HVDC engineering often does not operate at the rated power due to seasonal problems with loads and water sources. Therefore, by changing the power of HVDC

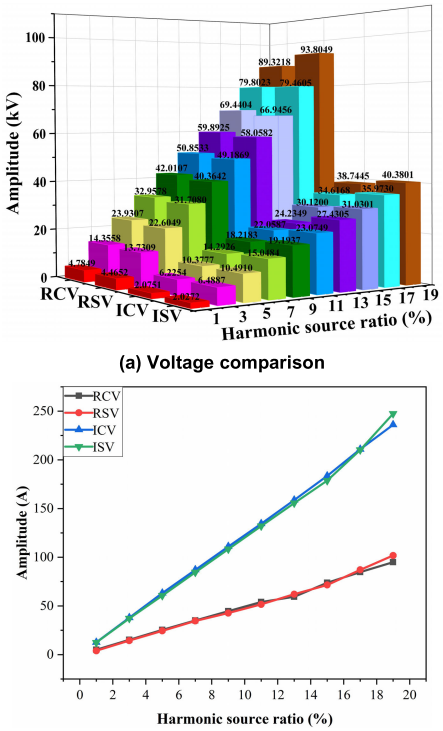

FIGURE 17. Comparison of the monopolar ground operation mode.

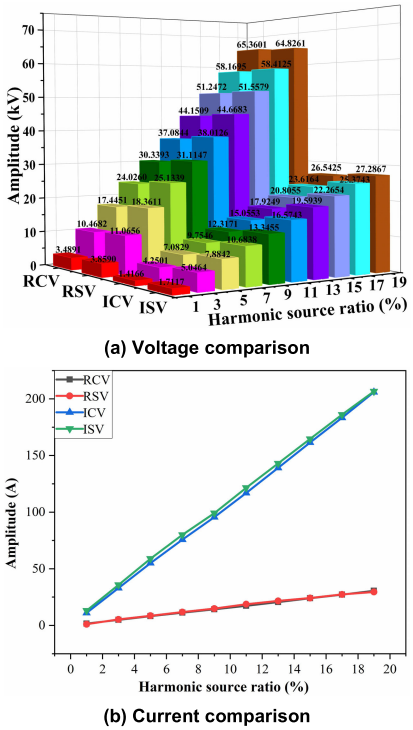

FIGURE 18. Comparison of the monopolar metallic operation mode.

transmission, it is important to investigate whether the HVDC transmission power has an influence on the transmission of harmonics in the DC line.

TABLE 7. Current transfer for different transmission powers.

(a)(Bipolar ground operation mode)

Power/ p.u.	CV/SV	Rectifier-side I/A	Inverter-side I/A	Amplification factor
0.1	CV	14.6828	123.5156	8.4122
	SV	16.2229	128.0629	7.8939
0.3	CV	15.1556	126.1072	8.3208
	SV	16.2475	131.0056	8.0630
0.5	CV	15.9798	131.9749	8.2588
	SV	18.6376	132.6986	7.1199
0.7	CV	16.6396	136.2520	8.1884
	SV	15.8586	139.7589	8.8127
0.9	CV	17.2450	139.4589	8.0869
	SV	19.4852	139.9095	7.1802

(b)(Monopolar metallic operation mode)

Power/ p.u.	CV/SV	Rectifier-side I/A	Inverter-side I/A	Amplification factor
0.1	CV	13.4188	89.5638	6.6745
	SV	14.7955	95.6183	6.4626
0.3	CV	13.6418	91.4308	6.7022
	SV	13.0580	98.4063	7.5360
0.5	CV	13.7230	92.0464	6.7074
	SV	13.3338	97.1972	7.2895
0.7	CV	14.1836	95.2913	6.7184
	SV	13.8889	101.2777	7.2919
0.9	CV	14.1269	95.2956	6.7457
	SV	14.2129	99.8798	7.0273

The harmonic amplitude and position are the same as in the previous section. The voltage and current components on both sides are recorded when the HVDC power is between 0.1 p.u. and 0.9 p.u. By comparing the calculated value (CV) with the simulated value (SV), the effects of the HVDC transmission power on the harmonic transfer amplification are analyzed while also further verifying the accuracy of the model.

The current CV and SV of the monopolar ground operation mode are shown in TABLE 3. The details of the other two operating modes are shown in APPENDIX E.

As the power changes, the current component changes, but the change is not large. The current amplification factor also changes little, and the value fluctuates around a fixed value. Thus, the magnitude of the current component is basically independent of the HVDC transmission power.

2) DC SMOOTHING REACTOR

The smoothing reactor is used to suppress the ripple in the DC voltage after rectification and is one of the important pieces of equipment of the converter station. Therefore, it is especially

TABLE 8. Current transfer for different smoothing reactors.

(a)(Bipolar ground operation mode)

L/H	CV/SV	Rectifier-side I/A	Inverter-side I/A	Amplification factor
0.25	CV	9.9410	143.9091	14.4776
	SV	12.2654	144.3162	11.7660
0.30	CV	18.2046	144.0716	7.9140
	SV	19.8142	146.5658	7.3969
0.35	CV	27.7143	149.3925	5.3904
	SV	30.0384	148.9573	4.9588
0.40	CV	37.7900	153.8053	4.0700
	SV	9.9389	143.9107	14.4794

(b)(Monopolar ground operation mode)

L/H	CV/SV	Rectifier-side I/A	Inverter-side I/A	Amplification factor
0.25	CV	38.6487	106.4351	2.7539
	SV	36.4756	104.8240	2.8738
0.30	CV	44.6024	111.0193	2.4891
	SV	42.6339	108.3050	2.5403
0.35	CV	54.8730	124.0967	2.2615
	SV	48.7842	111.9172	2.2941
0.40	CV	58.1083	120.0628	2.0662
	SV	56.9377	117.2353	2.0590

important to analyze the influence of the smoothing reactor on the harmonic transfer amplification.

The harmonic conditions are the same as before. The voltage and current components on both sides are recorded by modifying the value of the smoothing reactor from 0.25 H to 0.4 H. The current CV and SV of the monopolar metallic operation mode are shown in TABLE 4. The details of the other two operating modes are shown in APPENDIX F.

From the data in the table, it can be found that, as the DC smoothing reactor increases, the current component also increases. However, the amplification of the current decreases as the smoothing reactor increases. Thus, the smoothing reactor has an inhibitory effect on the amplification of the harmonics.

VI. CONCLUSION

In this paper, a two-port unified model is proposed. The transformer, converter, smoothing reactor and filter, and DC line in the HVDC transmission system are equivalent to one two-port network. In different operating modes of HVDC transmission, only the connection mode of the two ports needs to be modified. By a comparison with detailed HVDC model simulation results of PSCAD/EMTDC, the conclusions can be drawn as follows:

1) The two-port unified model is a computationally inexpensive option for the analysis of the harmonics of an LCC-HVDC system, due to the small computational burden and improved efficiency. By comparing the results with a simulation, it is found that the CV based on the proposed model are basically consistent with the simulation results for different operation modes, and the accuracy and practicability of the method are illustrated.

2) An analysis of harmonic transfer and amplification are presented by the established two-port unified model. The results show that harmonic transmission and amplification have little to do with the HVDC operating parameters (transmission power) but are closely related to the HVDC system parameters (DC smoothing reactor).

3) All the results show that the two-port unified model can be applied to the assessment of the harmonic current in the initial stage of HVDC project planning. The assessment parameter has a certain reference value for an actual HVDC transmission system and can provide a reference basis for the formulation of a harmonic protection strategy.

However, due to the time-varying nature of the converter, there are certain errors in the quantitative calculation. Therefore, accurately constructing the equivalent circuit of the converter in a quantitative calculation will be the focus of further research and very significant work.

APPENDIXES

APPENDIX A

See TABLE 5.

APPENDIX B

See FIGURE 16.

APPENDIX C

See TABLE 6.

APPENDIX D

See FIGURES 17 and 18.

APPENDIX E

See TABLE 7.

APPENDIX F

See TABLE 8.

REFERENCES

[1] E. Hossain, M. R. Tur, S. Padmanaban, S. Ay, and I. Khan, "Analysis and mitigation of power quality issues in distributed generation systems using custom power devices," *IEEE Access*, vol. 6, pp. 16816–16833, 2018.

[2] H. Yoshida and K. Wada, "Third–harmonic current suppression for power distribution systems under unbalanced installation of DG units," *IEEE Trans. Ind. Electron.*, vol. 62, no. 9, pp. 5578–5585, Sep. 2015.

[3] X. Wang, F. Blaabjerg, and W. Wu, "Modeling and analysis of harmonic stability in an ac power-electronics-based power system," *IEEE Trans. Power Electron.*, vol. 29, no. 12, pp. 6421–6432, Dec. 2014.

[4] Y. Z. Zhang and C. M. Bush, "Analysis and mitigation of interaction between transformer inrush current and HVDC operation," in *Proc. IEEE Power Energy Soc. Gen. Meeting*, Chicago, IL, USA, Jul. 2017, pp. 1–5.

[5] Y. Xue, X.-P. Zhang, and C. Yang, "Elimination of commutation failures of LCC HVDC system with controllable capacitors," *IEEE Trans. Power Syst.*, vol. 31, no. 4, pp. 3289–3299, Jul. 2016.

[6] A. Zheng, C. Guo, P. Cui, W. Jiang, and C. Zhao, "Comparative study on small–signal stability of LCC–HVDC system with different control strategies at the inverter station," *IEEE Access*, vol. 7, pp. 34946–34953, 2019.

[7] W. B. Cao, X. G. Yin, X. W. Qi, Y. X. Wang, W. Liu, and Y. L. Pan, "Analysis for DC transmission line harmonics originated from AC transformer inrush current and improved method for DC harmonic protection," *J. Eng.*, vol. 2019, no. 16, pp. 1056–1061, 2019.

[8] Z. K. Li, Z. G. Chen, G. Wang, and H. F. Li, "Analysis for DC transmission line harmonics originated from AC transformer inrush current and improved method for DC harmonic protection," in *Proc. Asia–Pacific Power Energy Eng. Conf.*, Wuhan, China, Mar. 2011, pp. 25–28.

[9] F. D. Marvasti and A. Mirzaei, "A novel method of combined dc and harmonic overcurrent protection for rectifier converters of monopolar HVDC systems," *IEEE Trans. Power Del.*, vol. 33, no. 2, pp. 892–900, Apr. 2018.

[10] Q. Wang, C. Zhang, X. Wu, and Y. Tang, "Commutation failure prediction method considering commutation voltage distortion and DC current variation," *IEEE Access*, vol. 7, pp. 96531–96539, 2019.

[11] Y. Z. Zhang and C. Bush, "Bush analysis and mitigation of interaction between transformer inrush current and HVDC operation," in *Proc. IEEE Power Energy Soc. Gen. Meeting*, Chicago, IL, USA, Jul. 2017, pp. 1–5.

[12] S. Luo, X. Dong, S. Shi, and B. Wang, "A directional protection scheme for HVDC transmission lines based on reactive energy," *IEEE Trans. Power Del.*, vol. 31, no. 2, pp. 559–567, Apr. 2016.

[13] M. Daryabak, S. Filizadeh, J. Jatskevich, A. Davoudi, M. Saeedifard, V. K. Sood, J. A. Martinez, D. Aliprantis, J. Cano, and A. Mehrizi-Sani, "Modeling of LCC–HVDC Systems using dynamic phasors," *IEEE Trans. Power Del.*, vol. 29, no. 4, pp. 1989–1998, Aug. 2014.

[14] C. Guo, A. Zheng, Z. Yin, and C. Zhao, "Small-signal stability of hybrid multi-terminal HVDC system," *Int. J. Electr. Power Energy Syst.*, vol. 109, pp. 434–443, Jul. 2019.

[15] L. H. Hu and R. Yacamini, "Harmonic transfer through converters and HVDC links," *IEEE Trans. Power Electron.*, vol. 7, no. 3, pp. 514–525, Jul. 1992.

[16] S. Chen, A. Wood, and J. Arrillaga, "HVDC converter transformer core saturation instability: A frequency domain analysis," *IEE Proc.-Gen. Transmiss. Distrib.*, vol. 143, no. 1, pp. 75–81, 1996.

[17] Y. Qi, H. Zhao, S. Fan, A. M. Gole, H. Ding, and I. T. Fernando, "Small signal frequency–domain model of a LCC–HVDC converter based on an infinite series–converter approach," *IEEE Trans. Power Del.*, vol. 34, no. 1, pp. 95–106, Feb. 2019.

[18] C. Guo, W. Liu, J. Zhao, and C. Zhao, "Impact of control system on small-signal stability of hybrid multi-infeed HVDC system," *IET Gener., Transmiss. Distrib.*, vol. 12, no. 19, pp. 4233–4239, Oct. 2018.

[19] C. Y. Guo, C. Y. Zhao, R. Iravani, H. Ding, and X. L. Wang, "Impact of phase locked loop on small-signal dynamics of the line commutated converter based high voltage direct current station," *IET Gener., Transmiss. Distrib.*, vol. 11, no. 5, pp. 1311–1318, 2017.

[20] W. Gang, L. Zhikeng, L. Haifeng, L. Xiaolin, and F. Chuang, "HVDC converter modeling and harmonic calculation under asymmetric faults in the AC system," in *Proc. IEEE Power Energy Soc. Gen. Meeting*, Jul. 2009, pp. 1–6.

[21] A. Bagheri-Vandaei and S. Filizadeh, "Generalised extended-frequency dynamic phasor model of LCC–HVDC systems for electromagnetic transient simulations," *IET Gener., Transmiss. Distrib.*, vol. 12, no. 12, pp. 3061–3069, Jul. 2018.

[22] M. Daryabak, S. Filizadeh, and A. B. Vandaei, "Dynamic phasor modeling of LCC-HVDC systems: Unbalanced operation and commutation failure," *Can. J. Electr. Comput. Eng.*, vol. 42, no. 2, pp. 121–131, Jun. 2019.

[23] L. H. Hu and R. Yacamini, "Calculation of harmonics and interharmonics in HVDC schemes with low DC side impedance," *IEEE Trans. Power Electron.*, vol. 140, no. 6, pp. 514–525, Nov. 1993.

[24] R. Carbone, F. Derosa, R. Langella, and A. Testa, "A new approach for the computation of harmonics and interharmonics produced by line–commutated AC/DC/AC converters," *IEEE Trans. Power Del.*, vol. 20, no. 3, pp. 2227–2234, Jul. 2005.

[25] F. Wang, Z. Xu, and Y. Huang, "DC harmonic current calculation for HVDC systems based on the classical transmission line model," in *Proc. IEEE Int. Conf. Power Syst. Technol.*, Hangzhou, China, Oct. 2010, pp. 1–5.

[26] J. Liu, G. Wang, H. F. Li, T. L. Ding, and Z. K. Li, "HVDC harmonic calculation under asymmetric faults in the AC system based on particle swarm optimization," in *Proc. Int. Conf. Adv. Power Syst. Autom. Protection*, Beijing, China, Oct. 2011, pp. 584–589.

[27] G. Bathurst, B. Smith, N. Watson, and J. Arrillaga, "Modelling of HVDC transmission systems in the harmonic domain," *IEEE Trans. Power Del.*, vol. 14, no. 3, pp. 1075–1080, Jul. 1999.

[28] V. K. Sood, *HVDC and FACTS Controllers-Applications of Static Converters in Power Systems*. Norwell, MA, USA: Kluwer Academic, 2004, pp. 10–13.

[29] Y. Huang, Q. M. Xin, X. B. Zhao, Y. X. Lu, and L. Guo, "Research on fast conversion method of metallic return to earth return operation mode in HVDC system," in *Proc. Int. Conf. Power Syst. Technol.*, Guangzhou, China, Nov. 2018, pp. 1–5.

[30] Y. W. Huang, L. H. Dong, S. Ebrahimi, N. Amiri, and J. Jatskevich, "Dynamic phasor modeling of line commutated rectifiers with harmonics using analytical and parametric approaches," *IEEE Trans. Energy Convers.*, vol. 32, no. 2, pp. 534–547, Jun. 2017.

[31] G. Wang, Z. L. Li, H. F. Li, and X. X. C. Li; Fu, "Modeling of the HVDC convertor using dynamic phasor under asymmetric faults in the AC system," in *Proc. Int. Conf. Sustain. Power Gener. Supply*, Nanjing, China, Apr. 2009, pp. 1–5.

[32] C. Liu, A. Bose, and P. Tian, "Modeling and analysis of HVDC converter by three–phase dynamic phasor," *IEEE Trans. Power Del.*, vol. 29, no. 1, pp. 3–12, Feb. 2014.

[33] L. Hu and R. Morrison, "The use of modulation theory to calculate the harmonic distortion in HVDC systems operating on an unbalanced supply," *IEEE Trans. Power Syst.*, vol. 12, no. 2, pp. 973–980, May 1997.

[34] J. Marti, "Accurate modelling of frequency–dependent transmission lines in electromagnetic transient simulations," *IEEE Trans. Power Appar. Syst.*, vols. PAS–101, no. 1, pp. 147–157, Jan. 1982.

[35] Y. Zhang, Y. Li, J. Song, B. Li, and X. Chen, "A new protection scheme for HVDC transmission lines based on the specific frequency current of DC filter," *IEEE Trans. Power Del.*, vol. 34, no. 2, pp. 420–429, Apr. 2019.

[36] M. Szechtman, T. Wess, and C. V. Thio, "First benchmark model for HVDC control studies," *Electra*, vol. 135, no. 4, pp. 55–75, Apr. 1991.

[37] J. Lu, X. Yuan, J. Hu, M. Zhang, and H. Yuan, "Motion equation modeling of LCC-HVDC station for analyzing DC and AC network interactions," *IEEE Trans. Power Del.*, early access.

[38] E. W. Kimbark, *Direct Current Transmission*. New York, NY, USA: Wiley, 1971, pp. 20–50.

[39] A. Yogarathinam, J. Kaur, and N. R. Chaudhuri, "Impact of inertia and effective short circuit ratio on control of frequency in weak grids interfacing LCC–HVDC and DFIG–based wind farms," *IEEE Trans. Power Del.*, vol. 32, no. 4, pp. 2040–2051, Aug. 2017.

[40] P. Kundur, N. J. Balu, and M. G. Lauby, *Power System Stability and Control*. New York, NY, USA: McGraw-Hill, 1994, pp. 231–245.

[41] C. K. Alexander and M. N. Sadiku, *Fundamentals of Electric Circuits*, 6th ed. New York, USA: McGraw-Hill, pp. 853–905, 2015.

[42] G. Georgiev, I. Zicmane, E. Antonovs, and K. Sergey, "Elimination of nodes with voltage dependent load characteristics in electrical network models," in *Proc. 10th Int. Conf. Environ. Electr. Eng.*, Rome, Italy, May 2011, pp. 1–5.

[43] J. J. Grainger and W. D. Stevenson, *Power System Analysis*. New York, NY, USA: McGraw-Hill, pp. 53–65, 1994.

DUI LIU received the B.S. degree from China Three Gorges University, in 2014, and the M.S. degree from Fuzhou University, in 2017. He is currently pursuing the Ph.D. degree with the South China University of Technology, Guangzhou, China. His research interests include power system fault analysis and HVDC transmission operation technology.

XIAOHUA LI (Member, IEEE) received the B.S. and Ph.D. degrees in electrical engineering from the Huazhong University of Science and Technology, China, in 1997 and 2003, respectively. She is currently a Professor with the School of Electric Power, South China University of Technology, mainly involved in power system fault analysis, relay protection, and HVDC power transmission operation research.

ZEXIANG CAI was born in Nanjing, China, in 1960. He received the bachelor's degree in electrical engineering from the Huainan Mineral Institute, Hefei, China, in 1982, the master's degree in electrical engineering from the Northeast China Institute of Electrical Power Engineering, in 1985, and the Ph.D. degree in electrical engineering from Tsinghua University, Beijing, China, in 1991. He is currently a Professor with the School of Electric Power Engineering, South China University of Technology, Guangzhou, China. His current research interests include power system stability and control and power system protective relaying.